

# Even more efficient magic state distillation by zero-level distillation

Tomohiro Itogawa,<sup>1</sup> Yugo Takada,<sup>2</sup> Yutaka Hirano,<sup>2</sup> and Keisuke Fujii<sup>1, 2, 3, 4</sup>

<sup>1</sup>*School of Engineering Science, Osaka University,*

*1-3 Machikaneyama, Toyonaka, Osaka 560-8531, Japan*

<sup>2</sup>*Graduate School of Engineering Science, Osaka University,*

*1-3 Machikaneyama, Toyonaka, Osaka 560-8531, Japan*

<sup>3</sup>*Center for Quantum Information and Quantum Biology,*

*Osaka University, 1-2 Machikaneyama, Toyonaka 560-0043, Japan*

<sup>4</sup>*RIKEN Center for Quantum Computing (RQC), Hirosawa 2-1, Wako, Saitama 351-0198, Japan*

(Dated: March 8, 2024)

Magic state distillation (MSD) is an essential element for universal fault-tolerant quantum computing, which distills a high fidelity magic state from noisy magic states using ideal (error-corrected) Clifford operations. For ideal Clifford operations, it needs to be performed on the logical qubits and hence takes a large spatiotemporal overhead, which is one of the major bottlenecks for the realization of fault-tolerant quantum computers (FTQC). Here we propose zero-level distillation, which prepares a high fidelity logical magic state using physical qubits on a square lattice using nearest-neighbor two-qubit gates without using multiple logical qubits. The key idea behind is using the Steane code to distill a logical magic state by using noisy Clifford gates with error detection. Then the Steane code state is teleported or converted to the surface codes. By carefully designing such circuits fault-tolerantly, the error rate of the logical magic state scales  $\sim 100 \times p^2$  in terms of the physical error rate  $p$ . For example, with a physical error rate of  $p = 10^{-4}$  ( $10^{-3}$ ), the logical error rate is reduced to  $p_L = 10^{-6}$  ( $10^{-4}$ ), resulting in an improvement of two (one) orders of magnitude. This contributes to reducing both space and time overhead for early FTQC as well as full-fledged FTQC combined with conventional multi-level distillation protocols.

## I. INTRODUCTION

Quantum computers are expected to provide advantages in solving problems that are intractable for classical computers such as prime factorization [1], linear system solver [2], and quantum chemistry [3]. Significant experimental efforts have been dedicated to the realization of quantum computers based on various physical systems. Among these, the superconducting system is one of the most promising candidates, and systems with 50-100 qubits have already been experimentally demonstrated [4, 5]. These quantum computers are called noisy intermediate-scale quantum computers (NISQ) [6], whose noise level is still high and the number of qubits is still limited, are currently unable to run sophisticated quantum algorithms with theoretically proven quantum speedup. Although NISQ-aware algorithms are being developed [7], an ultimate solution to these problems is to protect quantum information by quantum error correction [8] to realize a fault-tolerant quantum computer (FTQC) [9].

The surface codes [10, 11] are one of the most promising approaches for a fault-tolerant quantum computer using superconducting qubits, since they can be implemented on a two-dimensional square lattice and have high noise resilience [12, 13]. In FTQC whole computation has to be performed fault-tolerantly, with quantum information encoded in the logical qubits. While Clifford gates are relatively easy to do so, non-Clifford gates, such as the  $T$  gate, are hard to execute fault-tolerantly [14]. Therefore, magic state distillation (MSD) [15] is employed to prepare a high fidelity magic state  $T|+\rangle$  from noisy ones,

which is hence used to implement the  $T$  gate via gate teleportation [16].

While MSD is a crucial operation for achieving universal quantum computation, it requires a large number of qubits, which is an obstacle to the realization of FTQC [17]. This is because in most MSD protocols distillation is performed by using logical qubits with concatenating QEC codes which have the transversality of the  $H$  gate or  $T$  gate. In order to mitigate this, a physical level distillation protocol has been proposed with error detection [18]. While this approach has great potential to reduce the physical overhead, it has not been used for resource estimation because of the lack of concrete implementation on an architecture compatible with the surface codes.

In this work, we propose *zero-level distillation* to prepare a high fidelity logical magic state using physical qubits and nearest-neighbor two-qubit gates on a square lattice. At first, a magic state is encoded into the Steane code non-fault-tolerantly. Then such a noisy magic state is verified by using the Hadamard test of the logical  $H$  gate. The logical magic state is teleported into the rotated or planar surface codes. In addition to the teleportation-based approach, we also develop a fault-tolerant code conversion from the Steane code to the surface code, which allows us to save the number of qubits further while the depth is increased.

Throughout these processes, the operations employed are single-qubit gates/measurements and nearest-neighbor two-qubit gates. Furthermore, any single-point error is detected by the syndrome measurements and Hadamard test, and hence the logical error rate scales  $\mathcal{O}(p^2)$  in the physical error rate  $p$ . Since we do not need

QEC codes for fault-tolerant logical Clifford gates, the spacial overhead is much smaller than the conventional MSDs. For a performance analysis, we fully simulate zero-level distillation circuits consisting of approximately 40 qubits reducing the number of qubits required for simulation to 23 qubits. As a result, zero-level distillation reduces the logical error rate of a magic state  $p_L$  to  $p_L \simeq 100 \times p^2$  by only using 25 physical depths for the rotated surface code (23 for the planar surface code). For example, in the case of  $p = 10^{-4}$  ( $p = 10^{-3}$ ), the logical error rate results in  $p_L = 10^{-6}$  ( $p_L = 10^{-4}$ ), while the success probability is fairly high, 70% (95%). In the context of early-FTQC architecture [19], the zero-level distillation facilitates a significant enhancement, increasing the reliability of non-Clifford gate operations by an order of magnitude of two, in contrast to a scenario without MSD. In the context of full-fledged FTQC, zero-level distillation combined with conventional multi-level distillation [20] allows us to save the number of physical qubits significantly to achieve a given accuracy by reducing the number of levels.

The rest of the paper is organized as follows. In Sec II, we provide a preliminary explanation of the Steane code and MSD. In Sec III, we provide a detailed description of our proposal, zero-level distillation. In Sec IV, we explain the protocol to convert the Steane code state to the rotated surface code directly. In Sec V, we present the outcomes of our numerical simulation. Then, Sec VI is devoted to a conclusion.

## II. PRELIMINARY

In this section, we preliminarily explain the Steane code and MSD based on the transversality of the Hadamard gate on it.

The Steane code is a  $[[7,1,3]]$  stabilizer code, which can correct an arbitrary single-qubit Pauli error and detect an arbitrary two-qubit Pauli error. Stabilizer generators are defined by  $XIXIXIX$ ,  $XXIIXXI$ ,  $XIXXIXI$ ,  $ZIZIZIZ$ ,  $ZZIIZZI$ ,  $ZIZZIZI$ , each of them corresponds to three colored faces in Fig. 1. On the Steane code, all Clifford gates can be implemented transversally, while non-Clifford gates such as the  $T$  gate cannot. However, by using the transversality of the Hadamard  $H$  gate, a special resource state, the so-called magic state can be prepared fault-tolerantly as follows.

A magic state  $|A\rangle$  is defined by  $|A\rangle \equiv e^{-i\frac{\pi}{8}Y} |+\rangle$ , which is an eigenstate of  $H$ . By using the transversality of  $H$  gate and controlled-Hadamard gates  $\Lambda(H)$ , we can implement a Hadamard test of the logical Hadamard operator followed by decoding as shown in Fig. 2 [21, 22], where the physical controlled-Hadamard gate  $\Lambda(H)$  is constructed by  $A^\dagger \Lambda(X) A$  from the CNOT gate  $\Lambda(X)$  and the non-Clifford gate  $A$ . Suppose that all Clifford gates are ideal, and only non-Clifford gates are subject to errors with a probability  $p$ , then the above Hadamard test of the logical Hadamard operator and decoding process

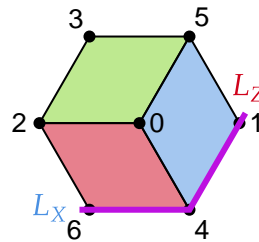


FIG. 1: The Steane code. A qubit is located at each vertex. The red, blue, and green faces represent stabilizers.

detects up to two errors and hence provides the magic state with error rate  $O(p^3)$ . In order to realize ideal Clifford gates, each qubit in Fig. 2 is further encoded into a logical qubit, and error-corrected Clifford gates are used. However, this approach costs a large amount of physical qubits and operations due to the concatenation of two QEC codes.

A lower-cost distillation method with flag qubits has been proposed by Goto [18]. This protocol works with noisy Clifford gates by carefully designing the circuit using flag qubits so that any single point of error introduced by the Clifford gates never ruins the distillation. Since this approach does not require logical qubits for the Clifford gates, it has the potential to significantly reduce the number of qubits required for MSD. However, the original proposal in Ref. [18] is based on the Steane code and all-to-all gate connectivity, which makes it difficult to apply for FTQC with the surface code on a nearest-neighbor architecture.

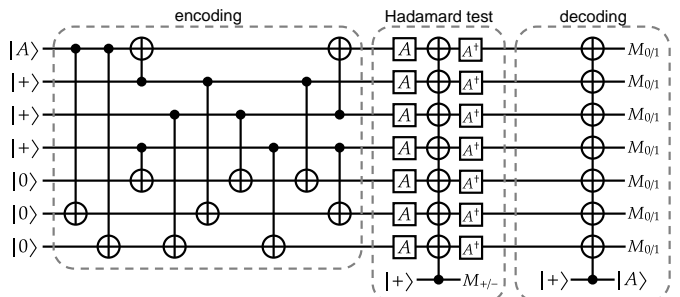


FIG. 2: MSD circuits based on transversality of the  $H$  gate. The encoding circuit creates a logical magic state encoded with the Steane code. The Hadamard test distills the magic state by measuring  $H^{\otimes 7}$ . The decoding circuit is based on the one-bit teleportation.

## III. ZERO-LEVEL DISTILLATION

In order to reduce the overhead for magic state distillation, we propose *zero-level distillation*, which is a protocol to prepare a logical magic state on the surface code

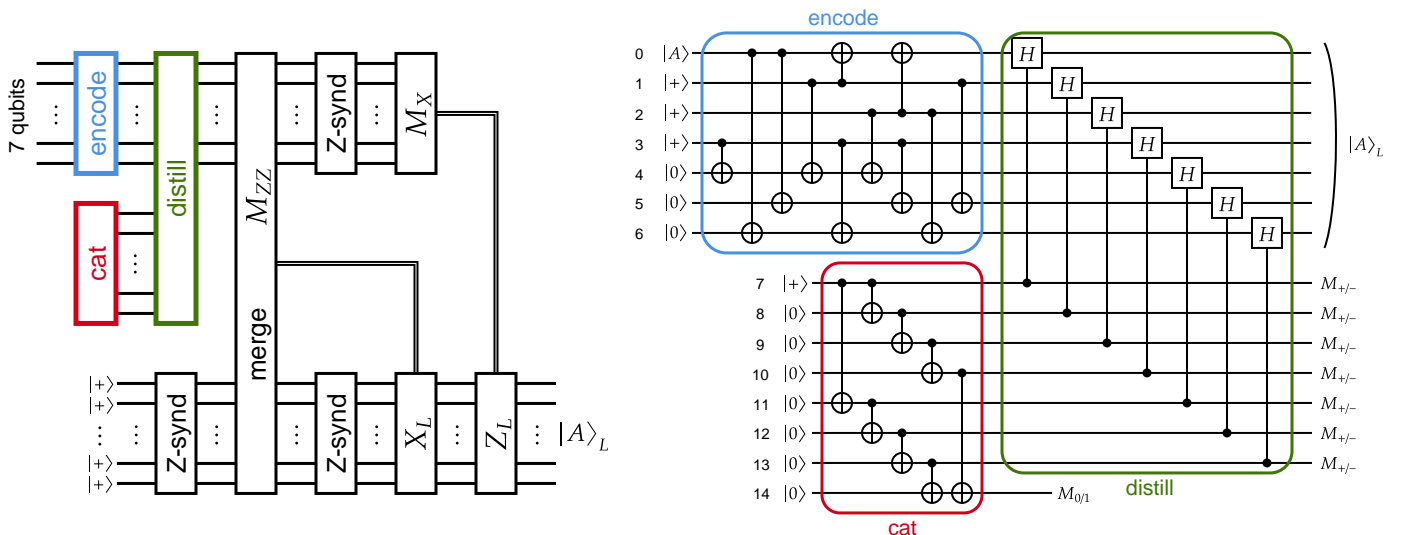


FIG. 3: (Left) The zero-level distillation circuit. (Right) The detailed circuits for encoding of noisy magic state, preparation of cat state, and distillation are shown. The circuit in the blue box encodes a magic state encoded with the Steane code non-fault-tolerantly. The circuit in the red box prepares a cat state. The circuit in the green box is the distillation circuit utilizing the Hadamard test.

without using multiple logical qubits. We perform physical level distillation using the Steane code by carefully designing the distillation circuit fault-tolerantly with a smaller number of physical qubits and nearest-neighbor two-qubit gates on the square lattice. Then, the logical magic state is teleported from the Steane code to the surface code, which can be viewed as lattice surgery between color and surface codes [23]. (In the next section, we will also provide another approach based on a code conversion from the Steane code to the surface code without teleportation.) This combination of two QEC codes allows us to prepare the logical magic state using a smaller number of physical qubits with high fidelity on the square lattice as seen below in detail.

Zero-level distillation consists of three key processes, non-fault-tolerant magic state encoding, post-selection with the Hadamard test, and teleportation-based injection with lattice surgery. The detailed steps are as follows (see schematic circuit diagram in Fig. 3):

- (i) Encode a magic state in the Steane code non-fault-tolerantly. In parallel, a 7-qubit cat state is also prepared.
- (ii) Execute distillation by the Hadamard test using the cat state. If the parity of the measurement outcome is even, the output state is accepted. In parallel, encode  $|+\rangle_L$  with the rotated surface code.
- (iii) Merge and split the magic state and  $|+\rangle_L$ , and perform the projection by the logical  $ZZ$  operator via the lattice surgery.
- (iv) Measure the  $Z$ -stabilizers on the Steane code and the surface code.

- (v) Measure qubits on the Steane code directly in  $X$ -basis to complete teleportation.

Fig. 3 shows the circuit for encoding noisy logical magic state and preparation of the cat state corresponding to step (i). The blue box in Fig. 3 shows the circuit for encoding a magic state non-fault-tolerantly with the Steane code. As shown in Fig. 4, the circuit can be constructed by using nearest-neighbor two-qubit gates on the square lattice. The red box in Fig. 3 shows the circuit for encoding a cat-state. While in the existing work [18] magic state distillation is executed using two ancilla qubits, the 7-qubit cat state is suitable in our situation where the qubit connectivity is very limited. Therefore, we use a 7-qubit cat state  $\frac{1}{\sqrt{2}}(|0\rangle^{\otimes 7} + |1\rangle^{\otimes 7})$  as ancilla qubits. This allows data and ancilla qubits to be adjacent on a square lattice as shown in Fig. 4 and 5.

In step (ii), the Hadamard test for the logical Hadamard gate is performed by using the cat state. The green box in Fig. 3 shows the distillation circuit with the Hadamard test, where the controlled-Hadamard gate  $\Lambda(H)$  is implemented as  $A^\dagger \Lambda(X) A$ . Fig. 6 (right) shows the details of the arrangement of qubits during distillation. Since data and ancilla qubits are located side by side, CNOT gates can be applied between them directly. After the logical controlled-Hadamard gate, the ancilla qubits from 7 to 13 in Fig. 3 are measured in the  $X$  basis. If the parity of the measurement outcomes is odd indicating any error, the distillation process is rejected. Otherwise, the output is accepted and proceeds to the next step. Then some qubits are moved for the lattice surgery as shown in Fig. 7(b). In parallel, the  $|+\rangle_L$  state is encoded with the rotated surface code by preparing  $|+\rangle$  states and measuring the  $Z$ -stabilizers as shown in Fig. 7(a).

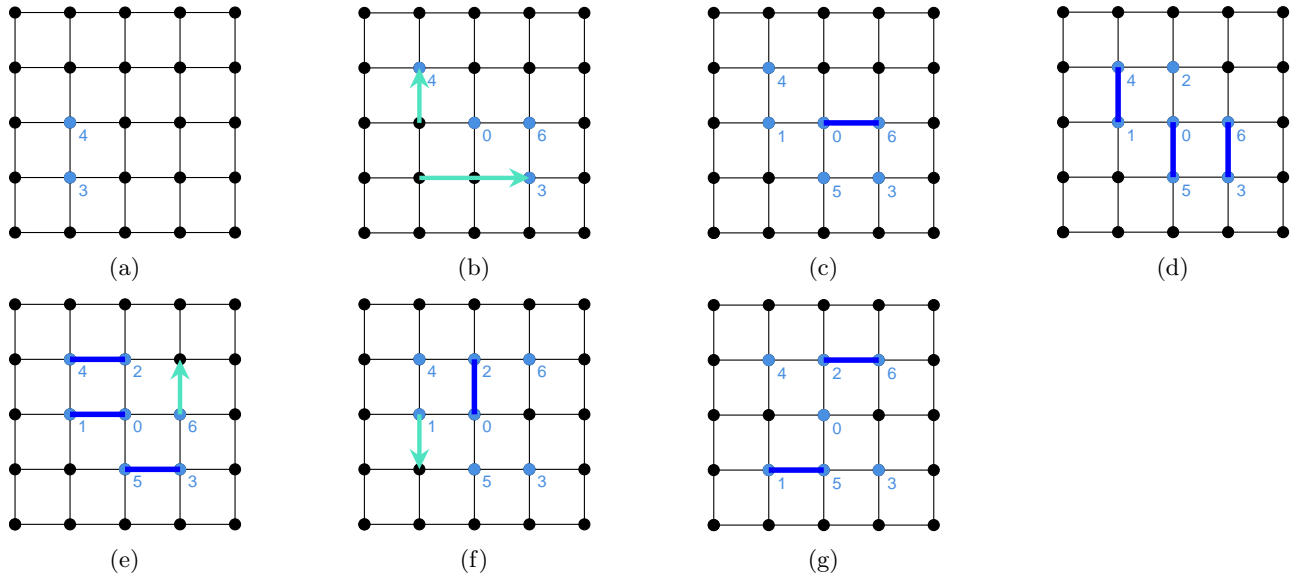


FIG. 4: Qubits arrangement during encoding a magic state. Each dot represents a qubit. The blue dots and numbers correspond to the locations of the qubits shown in Fig. 3. The light blue arrows indicate the transfer of qubits using one-bit teleportations. The blue lines indicate the application of CNOT gates.

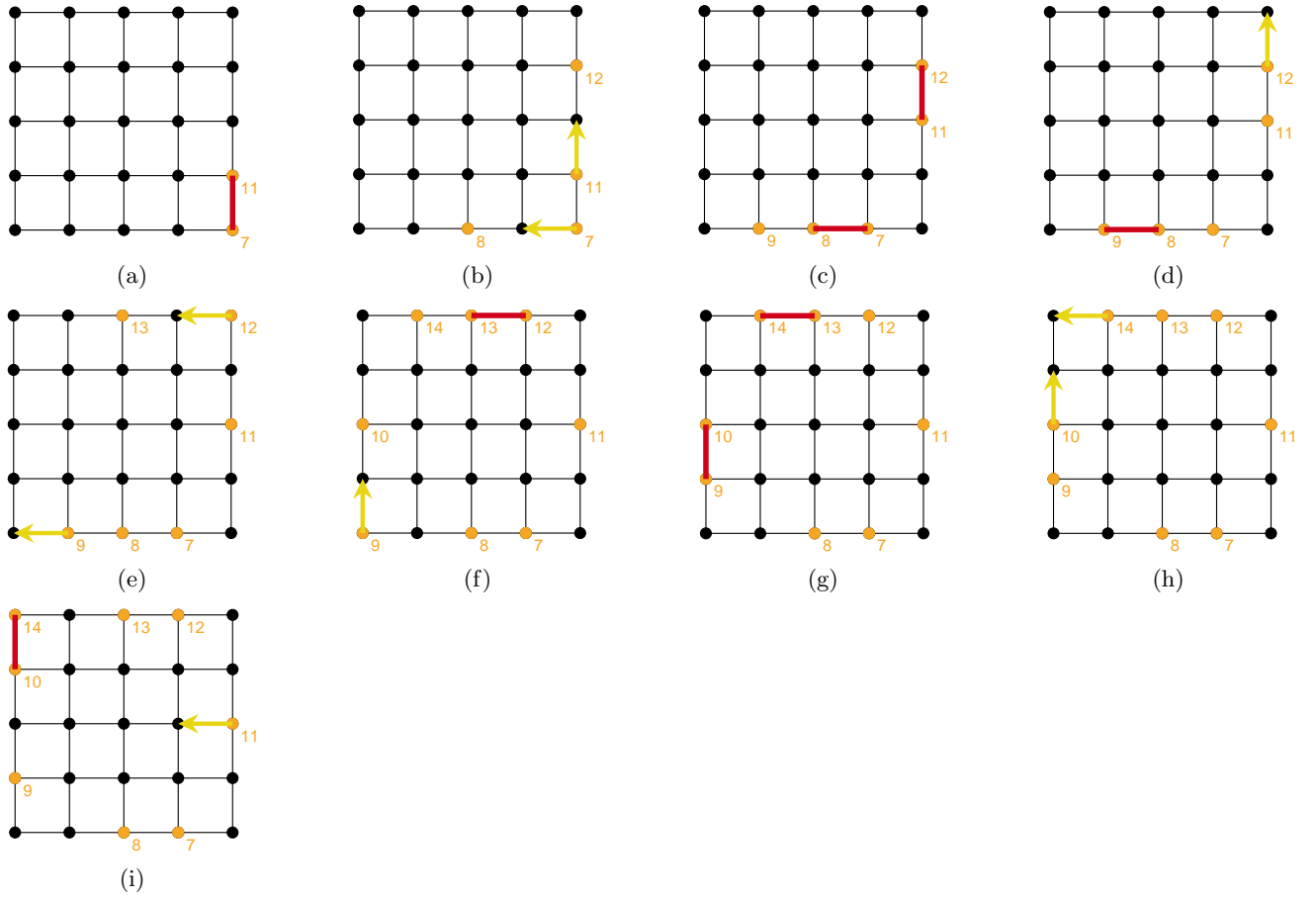


FIG. 5: Qubits arrangement during encoding a cat state. Each dot represents a qubit. The orange dots and numbers correspond to the locations of the qubits in Fig. 3. The yellow arrows indicate the transfer of qubits using one-bit teleportations. The red lines indicate the application of CNOT gates.

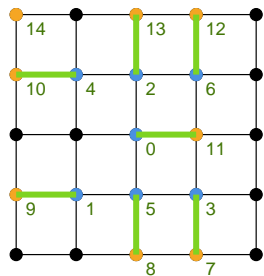


FIG. 6: Qubits arrangement during the Hadamard test. The blue and orange dots and numbers indicate the locations of the qubits shown in Fig. 3. A magic state is encoded in the blue qubits and a cat state is encoded in the orange qubits. The green lines indicate the CNOT gates.

In step (iii), Steane and rotated surface codes are merged as shown in Fig. 7(c) and then split via the lattice surgery. This results in projection with respect to  $L_Z^{\text{Steane}} \otimes L_Z^{\text{Surface}}$  since its eigenvalue can be obtained from the product of  $Z$ -type operators at the boundary shown by the purple area of Fig. 7(c). During the lattice surgery, it is necessary to measure the  $Z$ -stabilizers twice to detect measurement errors. If the measurement outcomes differ, such an event is rejected, and the protocol must be restarted from the beginning.

In step (iv),  $Z$ -stabilizers on the Steane code and the rotated surface code are measured. Fig. 8 illustrates the syndrome measurement circuits for the Steane code [24], where the ancilla qubits in Fig. 8 are represented by red, blue, or green dots in Fig. 7(d). The measurements detect two-qubit errors introduced during merging, as well as errors during magic state encoding or  $|+\rangle_L$  state encoding.

In step (v), each qubit in the Steane code is measured directly in the  $X$  basis to obtain the eigenvalue of the  $X$ -stabilizers and logical operators as shown in Fig. 7(d). Note that these eigenvalues should be interpreted appropriately according to the measurement outcome of the  $X$ -stabilizer at the boundary for splitting as usually done in the lattice surgery. This completes the teleportation of the distilled magic state on the Steane code to the rotated surface code. As usual, the Pauli frame of the logical qubit is updated according to the measurement outcome. Throughout all operations from the beginning, 25 physical depths are used. While we have demonstrated the proposed protocol for the rotated surface code, the planar surface code version is also shown in Appendix A.

#### IV. DIRECT CODE CONVERSION FROM STEANE TO SURFACE CODES

Here we present another protocol to prepare the logical magic state on the rotated surface code by converting the Steane code state to the rotated surface code directly without teleportation. This approach does not

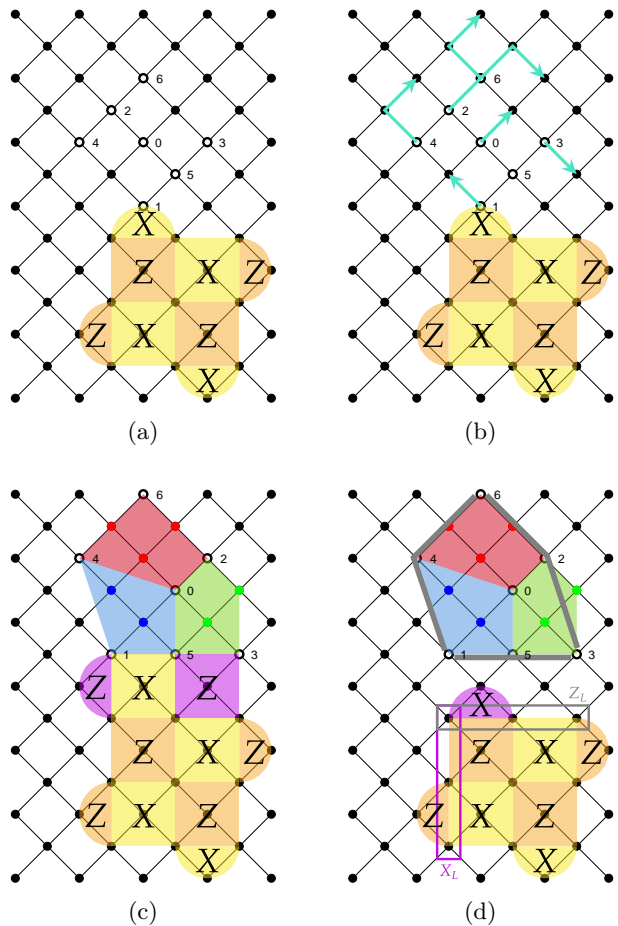


FIG. 7: Qubits arrangement and measurements during teleportation from the Steane code to the rotated surface code. The white dots and numbers indicate the locations of the qubits shown in Fig. 3, where the distilled magic state is encoded in the white qubits. The light blue arrows indicate the transfer of qubits using teleportation. The red, blue and green faces indicate the stabilizers of the Steane code, and the orange and yellow faces indicate the stabilizers of the rotated surface code. The purple faces indicate the  $Z$ -stabilizers for lattice surgery. The red, blue, and green dots are the ancilla qubits for the stabilizer measurements. The gray lines indicate logical operators of the Steane code. The purple box and the gray box indicate logical operators of the rotated surface code.

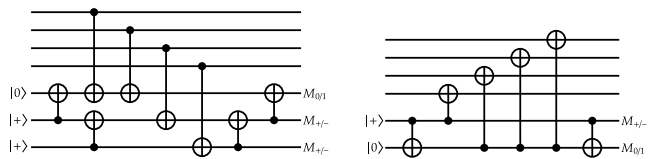


FIG. 8: The syndrome measurement circuits for the Steane code use three ancilla qubits (left) and two ancilla qubits (right), which correspond to red and blue/green in Fig. 7(d).

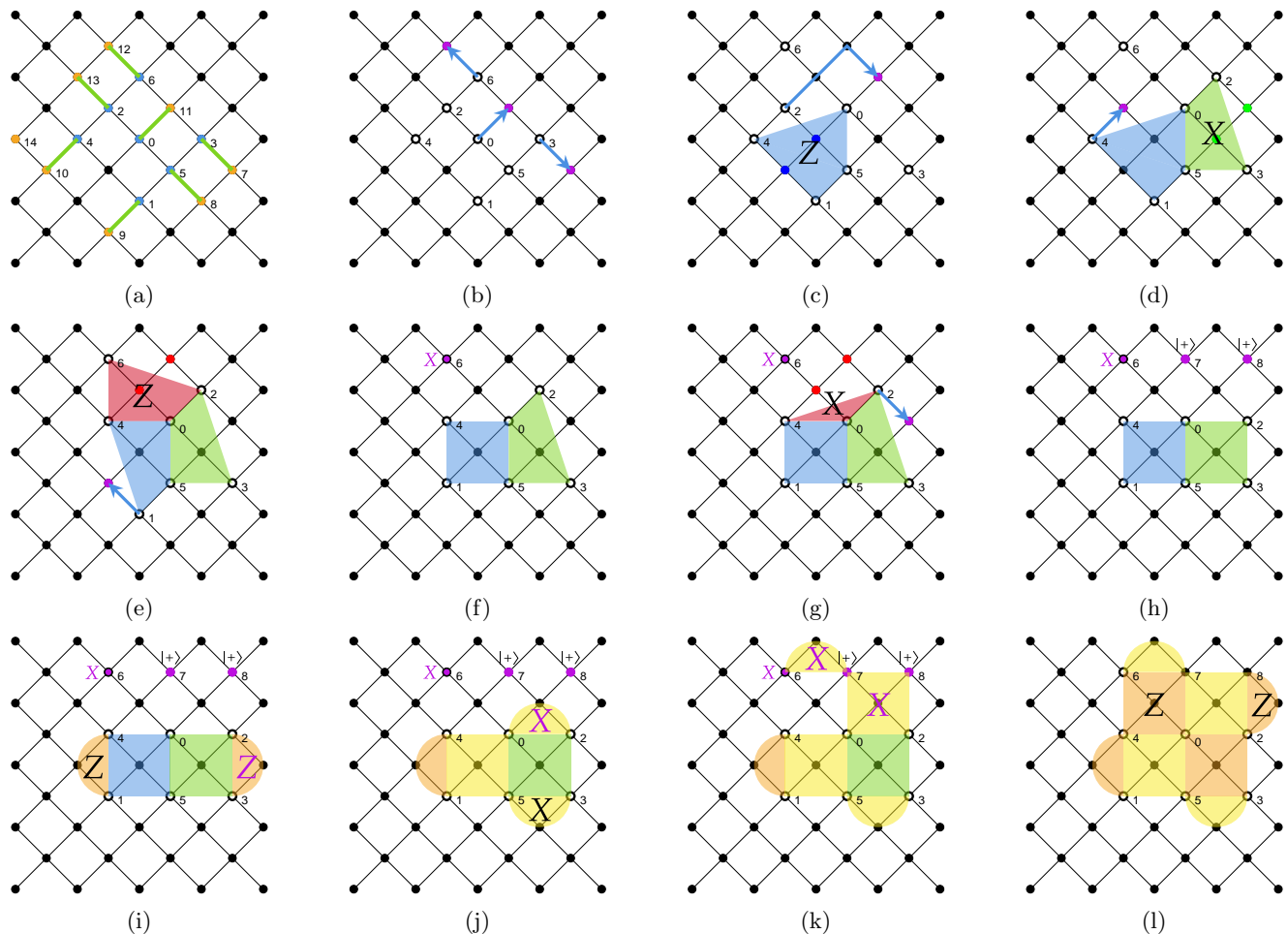


FIG. 9: Qubits arrangement and measurements during conversion from the Steane code to the rotated surface code. The blue and orange dots and numbers correspond to the locations of the qubits shown in Fig. 3. The blue arrows indicate the transfer of qubits using one-bit teleportations. The red, blue, and green faces indicate the stabilizers of the Steane code, and the orange and yellow faces indicate the stabilizers of the rotated surface code. The red, blue, and green dots are the ancilla qubits for the stabilizer measurements of the Steane code.

require the generation of two logical states and hence consumes fewer qubits compared to the teleportation-based approach above. As a drawback, the circuit depth is increased to 42, which is approximately twice as long as the teleportation-based approach. As a result, the logical error rate is worse than that of the teleportation method due to the strong influence of idling noise.

First, as shown in Fig. 9(a), a magic state is encoded as described in Sec III. After that, as shown in Fig. 9(b)–(l), we perform one-bit teleportations to move the qubits appropriately and stabilizer measurements to detect errors, and to form the stabilizer operators for the rotated surface codes. Specifically, Fig. 9(c)–(e) show  $Z$ ,  $X$ ,  $Z$ -stabilizer measurements respectively. If the syndrome values are odd in these three stabilizer measurements, the distillation process must be restarted from the beginning.

Next, we deform the Steane code to a 6-qubit code of distance two while keeping the logical state and fault-

tolerance. As shown in Fig. 9(f), qubit 6 is measured directly in the  $X$ -basis. The 6-qubit code consists of two  $X$  and  $Z$  weight-four stabilizers and one weight-three  $X$  stabilizer originating from the Steane code as shown in Fig. 9(g). Similar to the Steane code, the logical  $Z$  operator is composed of three qubits,  $Z_1Z_3Z_5$ . On the other hand, the logical  $X$  operator is composed of two qubits,  $X_1X_4$ . In Fig. 9(h), certain qubits are prepared in the  $|+\rangle$  states, which are used to form an  $X$  stabilizer of the rotated surface code later.

Finally, the 6-qubit code is deformed to the rotated surface code by measuring appropriate stabilizers with obtaining the syndrome values inherited from the Steane code as follows. In Fig. 9(i), two  $Z$ -type operators are measured; one is for the stabilizer for the rotated surface code and the other is to convert the  $X$ -type stabilizer of the Steane code (red face) into  $X$  stabilizers of the rotated surface code. The measurement outcomes of these two  $Z$ -type operators have to coincide since they

are linked by the blue and green stabilizers of the Steane code. Therefore, if the measurement outcomes disagree indicating any error, and hence the distillation process is rejected. Similarly, in Fig. 9(j), two  $X$ -type operators are measured to form the  $X$  stabilizers for the rotated surface code. If their measurement outcomes do not coincide, the distillation process is rejected. This measurement removes the  $Z$  stabilizer on the blue face, and only the  $X$  stabilizer is left (colored yellow). In Fig. 9(k), the  $X$ -stabilizers are measured to be formed, which is repeated twice to detect measurement errors. In Fig. 9(l) two  $Z$ -stabilizer stabilizers are measured and formed, which are repeated twice to detect measurement errors. This measurement removes the  $X$  stabilizer on the green face, and only the  $Z$  stabilizer is left (colored orange). This completes the code conversion and the magic state is now encoded in the rotated surface code. 42 physical depths are used to complete the code conversion including the magic state distillation part on the Steane code. Throughout this process, the Pauli frame should be updated based on the measurement outcomes as usual.

## V. NUMERICAL SIMULATION

We perform numerical simulation to verify zero-level distillation works fault-tolerantly and to estimate the logical error rate and success probability. Specifically, since our protocol includes non-Clifford gates, we employ a full vector simulation using Qulacs [25]. While the original circuits require about 40 qubits for the rotated surface code (50 for the planar surface code), we perform numerical simulations using only about 20 qubits by reusing the ancilla qubits without changing the structure of the original circuit [26]. In the case of the code conversion, 15 qubits are enough to simulate.

Regarding the noise model, each single-qubit and two-qubit gates are followed by single-qubit and two-qubit depolarizing noise with a probability  $p$ , respectively, where an idling process is also regarded as an identity gate and hence is followed by noise. In order to estimate the logical error rate  $p_L$ , the obtained magic state on the rotated surface code is virtually projected to the code space, and fidelity between the ideal magic state is calculated. If fidelity is not a unit, we count it as a logical error. The reason why we project the state to the ideal code space is to estimate the logical error rate by excluding potentially detectable errors. These detectable errors can be post-selected in the further process in the leading order by sacrificing a small amount of success probability.

The logical error rate  $p_L$  is estimated for various physical error rates  $p$ , where the numbers of samples are chosen to be  $10^6$  to  $10^7$ . The resultant logical error rate is shown in Fig. 10 for the cases of teleportation-based approaches for the planar (red) and rotated (blue) surface codes, and the code conversion approach (purple). We can see that the logical error rate scales like  $p_L = a \times p^2$  and the coefficient is 93.4 for the planar surface code and

106 for the rotated surface code. In the case of the code conversion, the coefficient is given by 199. Compared to the rotated surface code, the planar surface code has a slightly lower logical error rate due to less shuttling of qubits. The intersection of  $p_L \simeq 100p^2$  and  $p_L = p$  is located around  $p = 10^{-2}$ , which indicates that the logical error rate is improved by one order of magnitude at the times of  $p = 10^{-3}$  and by two orders of magnitude at the times of  $p = 10^{-4}$ . Compared to the teleportation-based approach, the code conversion provides a slightly higher logical error rate because of its large circuit depth.

The success probabilities of distillation are plotted as functions of the physical error rate  $p$  in Fig. 11 for the teleportation-based approaches of the planar surface code (red) and the rotated surface code (blue), and the code conversion (purple). The success rate is 70% when  $p = 10^{-3}$  and 95% when  $p = 10^{-4}$ , indicating that distillation succeeds with a high probability. Compared to the planar surface code, the rotated surface code has a slightly higher success probability since it uses less number of physical qubits. The success probability of the code conversion is almost the same as that of the planar surface code since it uses fewer number of physical qubits and gates.

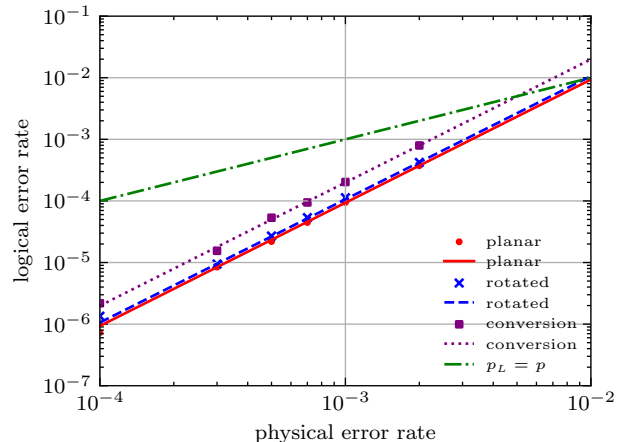


FIG. 10: The logical error rate  $p_L$  is plotted as a function of the physical error rate  $p$  for the teleportation-based approaches of the planar (red circle) and rotated (blue cross) surface code, and the code conversion (purple square). The red solid, blue dashed, and purple dotted lines are fitting with  $ap^2$ . The green dash-dotted line indicates  $p_L = p$ .

## VI. CONCLUSION AND DISCUSSION

We proposed zero-level distillation, which efficiently distills and prepares logical magic state encoded on the surface codes without using multiple logical qubits. All operations required can be implemented on the square lattice connectivity and the number of required physical

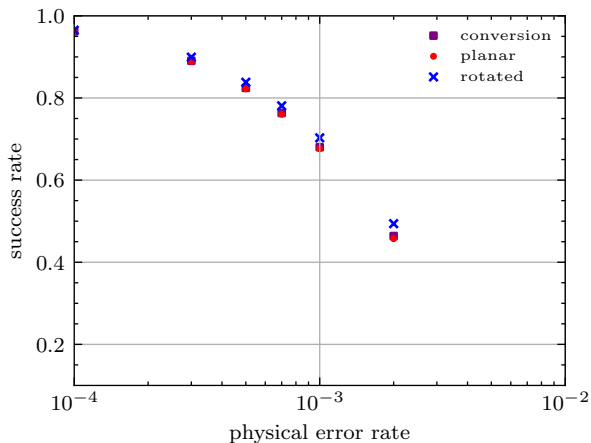


FIG. 11: The success rate is plotted as a function of the physical error rate  $p$  for the teleportation-based approaches of the planar (red circle) and rotated (blue cross) surface code, and the code conversion (purple square).

qubits is substantially reduced and spatial overhead for one or two logical patches is enough.

According to the numerical simulation, zero-level distillation with teleportation successfully reduces the logical error rate  $p_L$  of a logical magic state to  $p_L = 100 \times p^2$ . For example, when  $p = 10^{-3}$  and  $p_L = 10^{-4}$ , the logical error rates result in  $p = 10^{-4}$  and  $p_L = 10^{-6}$ , respectively indicating one and two orders of magnitude improvement. The success probability is reasonably high even when  $p = 10^{-3}$ . The depth of the zero-level distillation circuit is only 25, and hence it is compatible with the conventional multi-level distillation routines [20]. In addition, we also developed zero-level distillation based on the code conversion to further reduce the number of physical qubits employed.

Let us discuss how the proposed zero-level distillation has an impact when it is combined with further multi-level distillation. By changing the rotation axis, we can distill  $|T\rangle$  magic states with zero-level distillation. Such magic states can be used as level-1 magic states of multi-level distillation protocols generating  $|T\rangle$  magic states. For example, with  $p = 10^{-4}$ , zero-level distillation reduces the spatiotemporal overhead of two-level 15-to-1 distillation protocols in Ref. [20] achieving  $p_L = 1.5 \times 10^{-15}$  by more than 50%. A detailed analysis should be presented in future work. In addition to the non-Clifford gates, by using the transversality of  $S$  gate in the Steane code, we can also apply our protocol for preparing logical  $Y$  eigenstate reliably on the surface code, which could reduce the overhead for the logical  $S$  gate for the surface codes.

## ACKNOWLEDGMENTS

This work is supported by MEXT Quantum Leap Flagship Program (MEXT Q-LEAP) Grant No. JPMXS0118067394 and JPMXS0120319794, JST COI-NEXT Grant No. JPMJPF2014, and JST Moonshot R&D Grant No. JPMJMS2061.

### Appendix A: Zero-level distillation for the planar surface code

The magic state distilled on the Steane code can also be teleported to the planar surface code as well as the rotated surface code. In this case, the  $|+\rangle_L$  state encoded with the planar surface code and  $|+\rangle$  ancilla physical qubits are prepared in parallel with the Hadamard test as shown in Fig. 12(a). After the Hadamard test, some data qubits are moved as shown in Fig. 12(b). Then, as shown by the purple area of Fig. 12(c),  $L_Z^{\text{Steane}} \otimes L_Z^{\text{Surface}}$  is measured as a lattice surgery. During this lattice surgery, the  $Z$ -stabilizers have to be measured twice to detect measurement errors. As shown by the purple dots in Fig. 12(d), ancilla qubits on the boundary are measured in the  $X$  basis, which breaks the  $Z$ -stabilizers on the boundary, and two code states are split.

As shown in Fig. 12(d), the  $Z$  stabilizers are measured on both Steane and planar surface codes. Finally, the qubits on the Steane code are directly measured in the  $X$  basis to calculate the parities of  $X$ -stabilizers and logical operators. Throughout all operations from the beginning, 23 physical depths are used. Note that the Pauli frame has to be updated appropriately throughout these measurements as usual.



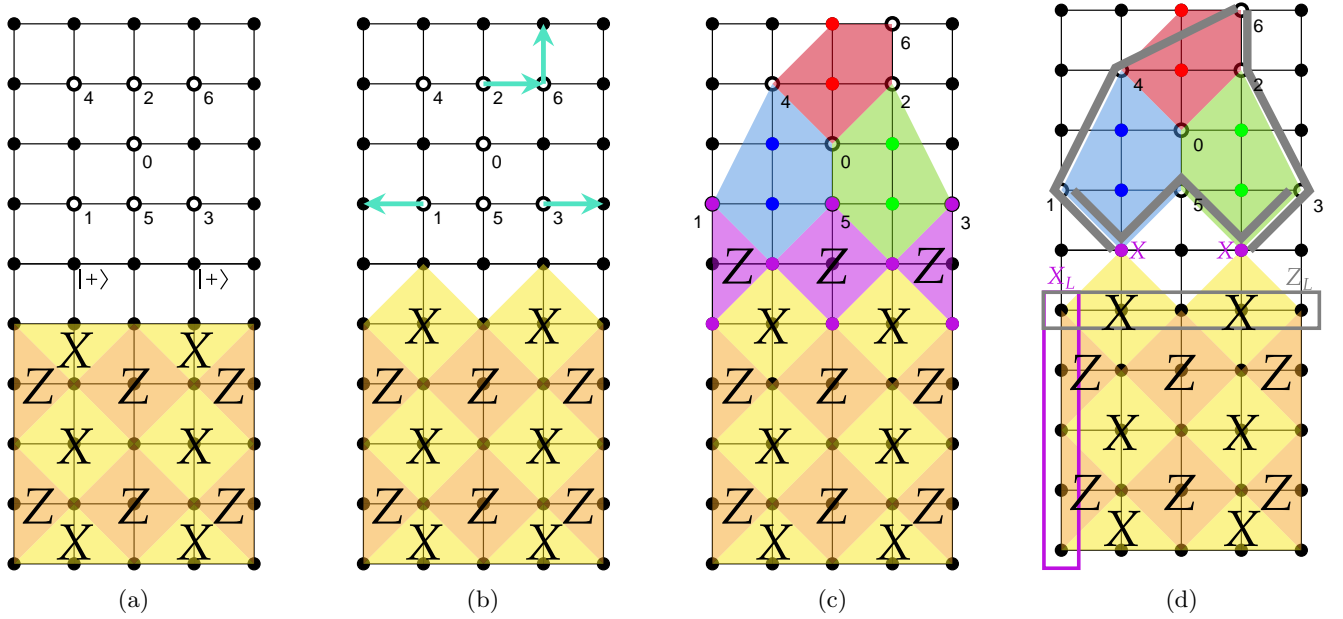


FIG. 12: Qubits arrangement and measurements during teleportation from the Steane code to the planar surface code. The white dots and numbers correspond to the locations of the qubits shown in Fig. 3, where the distilled magic state is encoded in the white qubits. The light blue arrows indicate the transfer of qubits using one-bit teleportations. The red, blue, and green faces indicate the stabilizers of the Steane code, and the orange and yellow faces indicate the stabilizers of the planar surface code. The red, blue, and green dots are the ancilla qubits for the stabilizer measurements of the Steane code. The purple faces indicate the Z-stabilizers at the boundary for the lattice surgery. The gray lines indicate logical operators of the Steane code. The purple box and the gray box indicate logical operators of the planar surface code.

- 
- [1] Peter W. Shor. Polynomial-time algorithms for prime factorization and discrete logarithms on a quantum computer. *SIAM Journal on Computing*, 26(5):1484–1509, 1997.
- [2] Aram W Harrow, Avinatan Hassidim, and Seth Lloyd. Quantum algorithm for linear systems of equations. *Physical review letters*, 103(15):150502, 2009.
- [3] Alán Aspuru-Guzik, Anthony D. Dutoi, Peter J. Love, and Martin Head-Gordon. Simulated quantum computation of molecular energies. *Science*, 309(5741):1704–1707, 2005.
- [4] A. Morvan et al. Phase transition in random circuit sampling, 2023.
- [5] Youngseok Kim, Andrew Eddins, Sajant Anand, Ken Xuan Wei, Ewout van den Berg, Sami Rosenblatt, Hasan Nayfeh, Yantao Wu, Michael Zaletel, Kristan Temme, and Abhinav Kandala. Evidence for the utility of quantum computing before fault tolerance. *Nature*, 618(7965):500–505, Jun 2023.
- [6] John Preskill. Quantum Computing in the NISQ era and beyond. *Quantum*, 2:79, August 2018.
- [7] M. Cerezo, Andrew Arrasmith, Ryan Babbush, Simon C. Benjamin, Suguru Endo, Keisuke Fujii, Jarrod R. McClean, Kosuke Mitarai, Xiao Yuan, Lukasz Cincio, and Patrick J. Coles. Variational quantum algorithms. *Nature Reviews Physics*, 3(9):625–644, Sep 2021.
- [8] Peter W Shor. Scheme for reducing decoherence in quantum computer memory. *Physical review A*, 52(4):R2493, 1995.
- [9] Keisuke Fujii. Quantum computation with topological codes: from qubit to topological fault-tolerance, 2015.
- [10] A.Yu. Kitaev. Fault-tolerant quantum computation by anyons. *Annals of Physics*, 303(1):2–30, 2003.
- [11] Sergey Bravyi and Robert Raussendorf. Measurement-based quantum computation with the toric code states. *Phys. Rev. A*, 76:022304, Aug 2007.
- [12] Austin G. Fowler, Matteo Mariantoni, John M. Martinis, and Andrew N. Cleland. Surface codes: Towards practical large-scale quantum computation. *Phys. Rev. A*, 86:032324, Sep 2012.
- [13] Robert Raussendorf and Hans J. Briegel. A one-way quantum computer. *Phys. Rev. Lett.*, 86:5188–5191, May 2001.
- [14] Emanuel Knill Bryan Eastin. Restrictions on transversal encoded quantum gate sets. *Phys. Rev. Lett.* 102, 110502, 2009.
- [15] Sergey Bravyi and Alexei Kitaev. Universal quantum computation with ideal clifford gates and noisy ancillas. *Physical Review A*, 71(2):022316, 2005.
- [16] Daniel Gottesman and Isaac L. Chuang. Demonstrating the viability of universal quantum computation using teleportation and single-qubit operations. *Nature*, 402(6760):390–393, 1999.
- [17] Craig Gidney and Martin Ekerå. How to factor 2048 bit RSA integers in 8 hours using 20 million noisy qubits. *Quantum*, 5:433, April 2021.
- [18] Hayato Goto. Minimizing resource overheads for fault-tolerant preparation of encoded states of the steane code. *Scientific Reports volume 6, Article number: 19578*, 2016.
- [19] Yutaro Akahoshi, Kazunori Maruyama, Hirotaka Oshima, Shintaro Sato, and Keisuke Fujii. Partially fault-tolerant quantum computing architecture with error-corrected clifford gates and space-time efficient analog rotations, 2023.
- [20] Daniel Litinski. Magic State Distillation: Not as Costly as You Think. *Quantum*, 3:205, December 2019.
- [21] Emanuel Knill, Raymond Laflamme, and Wojciech H Zurek. Resilient quantum computation. *Science*, 279(5349):342–345, 1998.
- [22] Emanuel Knill, Raymond Laflamme, and Wojciech H Zurek. Resilient quantum computation: error models and thresholds. *Proceedings of the Royal Society of London. Series A: Mathematical, Physical and Engineering Sciences*, 454(1969):365–384, 1998.
- [23] Hendrik Poulsen Nautrup, Nicolai Friis, and Hans J. Briegel. Fault-tolerant interface between quantum memories and quantum processors. *Nature Communications*, 8(1):1321, 2017.
- [24] Lingling Lao and Carmen G Almudever. Fault-tolerant quantum error correction on near-term quantum processors using flag and bridge qubits. *Physical Review A*, 101(3):032333, 2020.
- [25] Yasunari Suzuki, Yoshiaki Kawase, Yuya Masumura, Yuria Hiraga, Masahiro Nakadai, Jiabao Chen, Ken M. Nakanishi, Kosuke Mitarai, Ryosuke Imai, Shiro Tamiya, Takahiro Yamamoto, Tennin Yan, Toru Kawakubo, Yuya O. Nakagawa, Yohei Ibe, Youyuan Zhang, Hirotugu Yamashita, Hikaru Yoshimura, Akihiro Hayashi, and Keisuke Fujii. Qulacs: a fast and versatile quantum circuit simulator for research purpose. *Quantum*, 5:559, 2021.
- [26] Mitsuki Katsuda, Kosuke Mitarai, and Keisuke Fujii. Simulation and performance analysis of quantum error correction with a rotated surface code under a realistic noise model. *Phys. Rev. Res.*, 6:013024, Jan 2024.